Evaluating the protecting effects of two consolidants applied on Pietra di Lecce limestone: A neutronographic study

Evaluating the protecting effects of two consolidants applied on Pietra di Lecce limestone: A neutronographic study

Luciana Randazzo[a,1], Valentina Venuti[b,1], Giuseppe Paladini[b,*], Vincenza Crupi[c], Domenico Majolino[b], Frédéric Ott[d], Michela Ricca[a], Natalia Rovella[a], Mauro Francesco La Russa[a]

[a]*Department of Biology, Ecology and Earth Science, University of Calabria, via Pietro Bucci cubo 12B piano 2, 87036, Arcavacata di Rende (CS), Italy.*

[b]*Department of Mathematical and Computer Sciences, Physical Sciences and Earth Sciences, University of Messina, Viale Ferdinando Stagno D'Alcontres 31, 98166 Messina, Italy.*

[c]*Department of Chemical, Biological, Pharmaceutical and Environmental Sciences, University of Messina, Viale Ferdinando Stagno D'Alcontres 31, 98166 Messina, Italy.*

[d] *Laboratoire Léon Brillouin, CEA Saclay, 91191 Gif-sur-Yvette Cedex, France.*

[1]These Authors contributed equally to this study.
[*]Corresponding author. E-mail address: gpaladini@unime.it (G.Paladini).

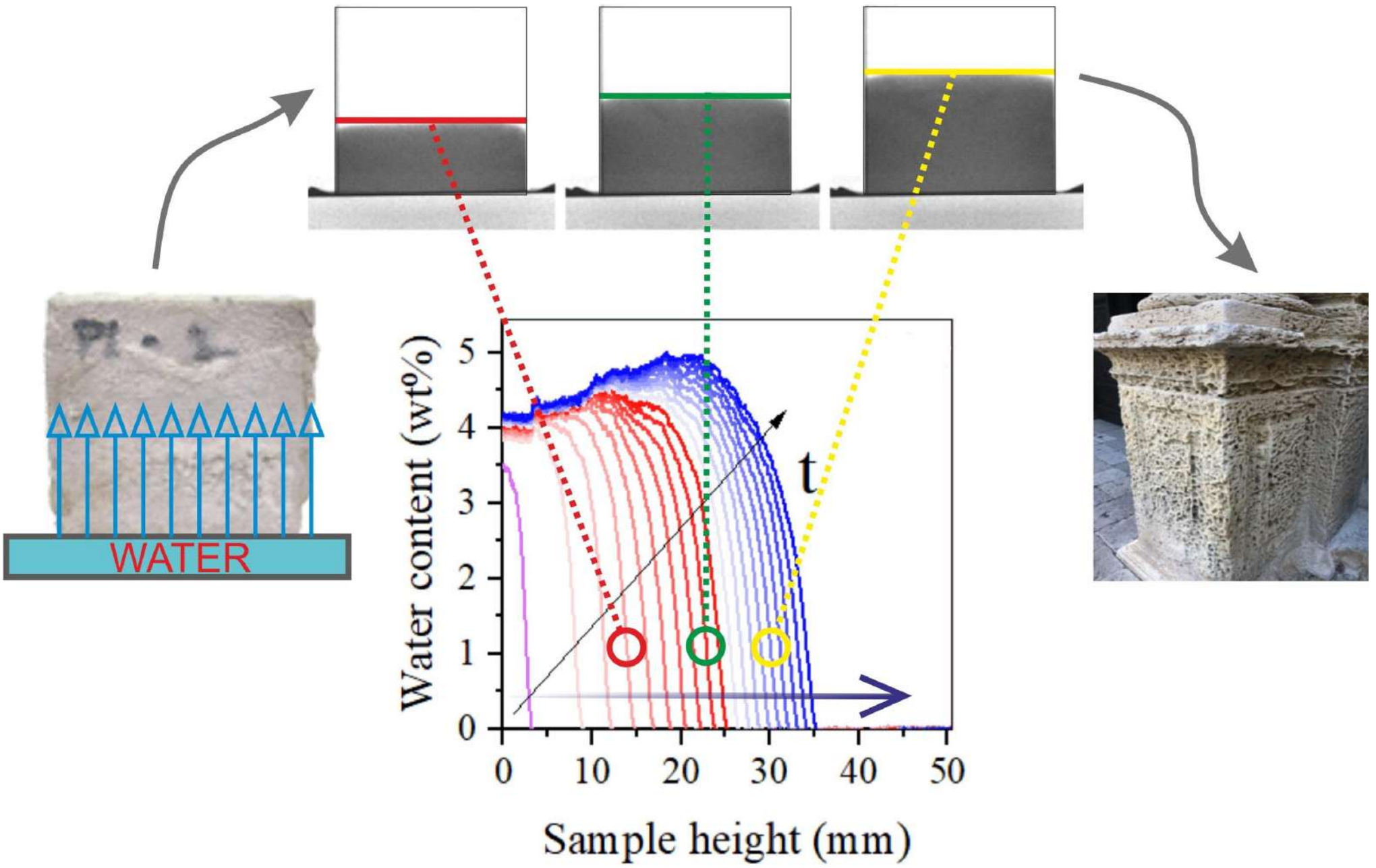
WATER
Water content (wt%)
Sample height (mm)
t
0
1
2
3
4
5
0
10
20
30
40
50

Evaluating the protecting effects of two consolidants applied on Pietra di Lecce limestone: A neutronographic study

Luciana Randazzo[a,1], Valentina Venuti[b,1], Giuseppe Paladini[b,*], Vincenza Crupi[c], Domenico Majolino[b], Frédéric Ott[d], Michela Ricca[a], Natalia Rovella[a], Mauro Francesco La Russa[a]

[a]*Department of Biology, Ecology and Earth Science, University of Calabria, via Pietro Bucci cubo 12B piano 2, 87036, Arcavacata di Rende (CS), Italy.*

[b]*Department of Mathematical and Computer Sciences, Physical Sciences and Earth Sciences, University of Messina, Viale Ferdinando Stagno D'Alcontres 31, 98166 Messina, Italy.*

[c]*Department of Chemical, Biological, Pharmaceutical and Environmental Sciences, University of Messina, Viale Ferdinando Stagno D'Alcontres 31, 98166 Messina, Italy.*

[d] *Laboratoire Léon Brillouin, CEA Saclay, 91191 Gif-sur-Yvette Cedex, France.*

[1]These Authors contributed equally to this study.
[*]Corresponding author. E-mail address: gpaladini@unime.it (G.Paladini).

Abstract

In this work a neutronographic investigation was carried out on a type of limestone, known as *Pietra di Lecce* stone, widely used in Italian Baroque as construction material. The limestone was treated with two different commercially-available coatings, namely nanosilica and nanolime, and artificially aged by temperature/relative humidity and salt crystallization. The aim was to provide an experimental evidence of the effectiveness of such protective coatings by looking at the water absorption process occurring inside the pore network of the analyzed stones. The analysis of the wetting front position revealed significant variations in the water absorption kinetics among the investigated samples, suggesting different mechanisms of interaction between the protective layer and the underlying bulk stone. Finally, a quantitative evaluation of the best effectiveness of the two products was addressed, particularly useful in view of an appropriate choice of restoration procedures to be applied to building materials.

Keywords: Limestone; Neutronography; Consolidants; Sorptivity; Water kinetics.

1. Introduction

One of the most relevant conservation principles in the field of cultural heritage states that historic objects or structures must be restored and preserved. Limestones represent the main type of stone materials around the world to be the subject of cultural heritage programs. Unfortunately, this kind of substrates undergo to different degradation and alteration processes, such as salts crystallization, erosion, dissolution, biological attack, etc. [1,2]. For this reason, in the last years, various consolidant and hydrophobic products have been widely used in the treatment of building materials of historical monuments, in view of consolidation and conservation of such structures [3-5]. To guarantee compatibility with the porous substrates, added products must be characterized by a suitable penetration depth with negligible or minimum alteration due to water permeability, and be stable along long times. Therefore, porosity and pore size distribution represent crucial parameters in conservation process, since they regulate the fluid mobility inside the material.

In particular, water dynamics in porous building materials represents a key tool for understanding the degradation processes due to both chemical and physical interactions between water and surrounding stone. As is well known, the rate of imbibitions, and hence the amount of water penetrating the porous material, can be considered simply proportional to the square root of the exposure time. Water diffusion into homogenous structures follows a classical behavior, although violation in the diffusion-like mechanism has often been achieved [6,7]. Such inconsistency must be associated to some kind of

processes occurring during the water suction, or to the presence of inhomogeneity within the inner structure of the investigated sample. Application of consolidants strongly affects the water motion, reducing the weathering effects to which buildings and monuments are continuously exposed.

The present study is part of a project having as goal the quantitative two- and three-dimensional textural compositional analysis of a variety of rocks at different scales from the microscopic to the macroscopic domain, aimed at the quantification of the fundamental properties such as porosity and pore size distribution, geochemistry, crystalline abundance, degradation attitude, etc.. Neutron and X-ray imaging techniques allow the analysis of different properties and processes including porosity, degradation effects, fluid mobility and penetration depth of protective and consolidant products [8-13]. In addition to diffraction and spectroscopic measurements, neutrons, beyond compositional and textural features of rocks, can observe as well variations and damages induced by both the application of different coatings and different aging tests in bulk samples, by static and dynamic neutron radiography (NR).

In this framework, neutronography was employed in order to investigate, in a completely non-invasive way, the interaction between two different protective/consolidant products, namely nanosilica (nano-SiO_2, NS) and nanolime ($Ca(OH)_2$, NL), and a type of limestone widely used in Italian Baroque buildings, i.e. *Pietra di Lecce* stone employed in Lecce city (Puglia, Southern Italy). Limestones under investigation were already characterized by mineralogical-petrographic and geochemical techniques [14-16]. Treated samples also underwent to different aging tests, such as temperature/relative humidity jumps and salt crystallization. Aim of the present study was to visualize the evolution of porosity, fracture network and rock disaggregation, also related to the texture microstructure, texture of the rocks and type of products used for their conservation. In the case of building stones, knowledge of these effects will help in elucidating their characteristics of durability and variation over time. Finally, we remark that, in this topic, the effects of protective and consolidant products are frequently limited to a qualitative description, whereas there are only few examples of studies providing a quantitative view, as the one proposed here.

2. Research Aim

In this work, neutronography was used to quantitatively and non-invasively study the variations of the porous structure, as a consequence of the application of different coatings having both consolidant and hydrophobic features, in a set of limestones cropping out in Lecce (Puglia, Southern Italy) and employed as building materials in Baroque historical monuments, also submitted to different aging tests. The performed research looks particularly promising in the field of Cultural Heritage, where the characterization of effects of coatings on building materials is necessary before selecting the appropriate restoration procedures.

3. Materials and Methods

3.1. Materials and preparation of test specimens

Pietra di Lecce (PL) stone is a fine-grained calcarenite, with a characteristic pale-yellow color. It is widely used in the Baroque heritage of the Salento area, as well as in minor buildings (Fig. 1).

Fig. 1. (a) Ancient quarry of *Pietra di Lecce* stone located in S. Cesario Street, Lecce; (b) Example of degradation forms suffered by *Pietra di Lecce* stone.

Petrographically, it is a wackestone [17], mainly composed of micritic fraction, mixed with fine clay minerals and poor cryptocrystalline calcitic cement; it contains fine microfossil fragments, grains of glauconite, sporadic quartz grains and phosphatic nodules [18,19]. The integral open porosity is around 40%, with pore radius mainly between 4 e 0.5 microns. The rock has around 80% of calcium carbonate and the insoluble residue is essentially made of clay minerals and glauconite. Before proceeding with the salt crystallization tests (artificial decay process), the samples were treated with two different consolidating products by brush application in order to verify their susceptibility to degradation. In particular, the commercial products chosen for the experimentation are: a) nanosilica suspension (Nano Estel®), and b) nanolime suspension (CaLoSiL®). The application of the consolidants was carried out on the surface of the stone samples (~ 5 × 5 × 2 cm^3) by brushing until they were getting saturation. Throughout the experimental phase, an untreated sample was used for subsequent comparison with the treated samples by subjecting it to the same procedure (see Table 1).

Sample Code	Products	Experimentation tests
PL1	Nano Estel®	Climatic chamber (T, RH) after 3 cycles of salt crystallization
PL2	Nano Estel®	Salt weathering (15 cycles)
PL3	Nano Estel®	Consolidated
PL4	CaLoSiL®	Climatic chamber (T, RH) after 3 cycles of salt crystallization
PL5	CaLoSiL®	Salt weathering (15 cycles)
PL6	CaLoSiL®	Consolidated
PL-TQ	Untreated	Not aged

Table 1. List of specimens and details about products and experimentation tests.

Both before and after treatments, some physical properties have been measured through the following techniques: colorimetric tests, scotch tape test and water absorption coefficient by capillarity [20]. Colorimetric test (CT) was performed by means of a CM-2600d Konica Minolta spectrophotometer, to evaluate chromatic variations induced by the treatment according to Normal 43/93. Chromatic values are expressed in the CIE L*a*b* space, L* being the lightness/darkness coordinate, a* the red/green coordinate (+a* indicating red and −a* green) and b* the yellow/blue coordinate (+b* indicating yellow and −b* blue). Scotch tape test (STT) is a method for making a quantified appraisal of the adhesion of a surface or a near to-surface layer to a substrate. According to [21], a pressure-sensitive tape was applied to the examined area and then removed. After each tape removal on the same area (for a total of 5 times), the weight of material detached from the surface was measured. Measurements were carried out on three samples for each treatment. The amount of materials removed from the surface of the stone should reflect the cohesion characteristics of the substrate. Therefore, an evaluation of the consolidation effects (after restoration procedures) as well as the surface degradation was achieved by using this test. After the consolidation of the stone and the

evaluation about the formulation's properties, the water absorption coefficient by capillarity was measured following the normative on three specimens for each treatment [20]. Then, untreated and treated specimens (three for each treatment) have undergone salt crystallization test to evaluate the weathering resistance of rock materials [22,23]. As far as salt crystallization is concerned, the procedure adopted is the one described in the existing standard [24], modified according to Benavente et al., 2001 [23]. Specifically, specimens underwent several crystallization cycles consisting of: a) 2 h of immersion in a supersaturated solution of sodium sulfate (14% w/w at 20 °C) for 10 % of their height, b) 8 h of drying in an oven at 45 °C, and c) 16 h of cooling at room temperature. The initial weight of each test sample was measured as well as the weight after each cycle; the resulting weight loss was therefore determined. Lastly, aging test by means of a climatic chamber has been carried out on specimens subjected to 3 cycles of salt crystallization test. The specimens held inside this temperature/humidity-controlled environment for 1500 hours, with a temperature variation between 20 °C and 45 °C and relative humidity from 40 to 80%. For laboratory experimentation, specimens of *Pietra di Lecce* stone were collected from quarries located in Salento area (Cursi-Lecce).

3.2. Neutron radiography and image processing

Neutron radiography measurements were carried out at the cold neutron imaging spectrometer IMAGINE of the Laboratoire Léon Brillouin (LLB) at the Orphée Reactor, in Saclay (F). Resolution was optimized by varying the L/D ratio, being L the distance between the entrance aperture of the neutron beam and the image plane, and D the diameter of the collimator aperture. Absorption contrast values with a resolution of 0.1% were achieved by increasing the L/D ratio up to 400, that guaranteed a spatial resolution of ~ 250 µm. The initial neutron flux was of about 2 x 10^7 neutrons × cm^{-2} × s^{-1}, that included a large spectrum of cold neutrons with wavelength ranging from 3 to 20 Å. Detection of the transmitted beam was achieved by using a sCMOS ANDOR NEO camera coupled to a Canon EFS 60mm F/2.8 Macro USM.

The acquired images allowed us to easily follow the water content profile because the key elements of the investigated limestones (Ca, C, O, etc.) are characterized by a cross section two orders of magnitude lower than hydrogen atoms in water. This means that even for low amount of penetrated water a good "contrast" between water and stone can be achieved.

First of all, dark field ($I_{(df)}$) and open beam ($I_{(ob)}$) images were acquired and used for further corrections. Limestones treated with the two coatings were placed one by one on a stack of filter paper within an aluminum container so that the whole stone specimen could be scanned. After the positioning, the water absorption dynamics by capillarity was recorded by manually adding water into the aluminum basement which ensured the saturation of the 10 mm thickness filter paper pack (obtained from Kaltek S.r.l. Padova Italy). Scans were acquired until full saturation of the specimen, with an exposure time of 10 s for all the investigated stones except than PL1, for which an exposure time of 40 s was used.

The images were pre- and post-processed using a homemade macro at the IMAGINE beamline. Accordingly, raw images of the dry ($I_{(dry)}$) and wet ($I_{(wet)}$) limestones were properly corrected with respect to both dark field ($I_{(df)}$) and open beam ($I_{(ob)}$) images using the following relations:

$$I_{(wet,corr)} = C\,\frac{I_{(wet)} - I_{(df)}}{I_{(ob)} - I_{(df)}} \tag{1}$$

and

$$I_{(dry,corr)} = C\,\frac{I_{(dry)} - I_{(df)}}{I_{(ob)} - I_{(df)}}\ , \tag{2}$$

where C is a rescaling factor which takes into account the neutron beam fluctuations. After that, images were uncontoured using a median filter in order to remove unwanted bright pixels mainly due to scattered γ-rays. Absolute transmission images of the samples were obtained with an absolute precision in the 1% range. The water absorption analysis was conducted by normalizing hydrated samples with respect to the steady-state dry images taken prior to the water absorption, in order to get images in which the contribution of the stone is removed and the measured transmission is directly related to the amount of water in the sample [25]. The same procedure was applied on a staircase-like sample holder containing twelve different water contents with standardized thickness, varying from 0.09 mm up to 5.00 mm. A plot of the neutron transmission vs. water thickness was created and used as a calibration curve for the water content of the water absorption images. The aforementioned procedure became necessary in the case of high values of water content, i.e. for equivalent thickness higher than 2.00 mm, where Beer-Lambert law is no more satisfied.

Pre-processing and image analysis were performed by using Fiji ImageJ (Fiji Is Just ImageJ - Image Processing and Analysis in Java, open source) [26].

Finally, the water content distribution inside the stones was quantified according to Kim et al. [27]. By dividing the obtained wet image ($I_{(wet,corr)}$) to the corresponding dry one ($I_{(dry,corr)}$), the 2D distribution of the water thickness ($\delta_w(x, y)$) can be written as:

$$\delta_w(x, y) = -\frac{\ln\left[I_{(wet,corr)}(x, y) \Big/ I_{(dry,corr)}(x, y) \right]}{\mu_w}. \quad (3)$$

In the above expression, $I_{(dry,corr)}(x, y) = I_0(x, y)e^{-\mu_s\delta_s}$ and $I_{(wet,corr)}(x, y) = I_0(x, y)e^{-(\mu_s\delta_s+\mu_w\delta_w)}$ respectively, being $I_0(x, y)$ the intensity of the incoming beam, μ_s and μ_w the stone and water attenuation coefficients, δ_s and δ_w the measured thickness of the stone and the equivalent water thickness.

Being the thickness of the stone known, the mean moisture content (MC) was first of all calculated by:

$$MC = \frac{\delta_w \cdot \rho_w}{\delta_s} \quad (4)$$

being ρ_w the density of water.

After that, the water content (WC), expressed in weight percentage, was determined as:

$$WC = \frac{MC}{\rho_s} \quad (5)$$

with ρ_s, the density of the stone, taken almost equal to 2.71 g/cm^3, being the stone mostly made up of calcite (90% of $CaCO_3$).

4. Results and Discussion

4.1. Colorimetric test, scotch tape test, water absorption coefficient by capillarity and salt crystallization test

Chromatic variations were evaluated to verify if a significant difference in color is present among treated and untreated samples, based on the normative [28]. Colorimetric tests results (Fig. 2(a)) indicate that the color change (ΔE) is mostly around 3-4 for samples treated with NS and these values may be considered satisfactory [29]. For samples treated with NL, becoming lighter, greener and bluer, the color differences are more enhanced. The scotch tape test (SST), carried out on PL-TQ, PL3 and PL6 stones as examples, furnished evidences on the superficial cohesion of the stone. The obtained results are shown in Fig. 2(b). The comparison between the mechanical features of treated samples with untreated ones highlighted an improvement in superficial cohesion of treated specimens that show a diminishing in released material. More specifically, specimen treated with NL gives a better result, showing an enhanced efficacy as far as increased cohesion properties are concerned.

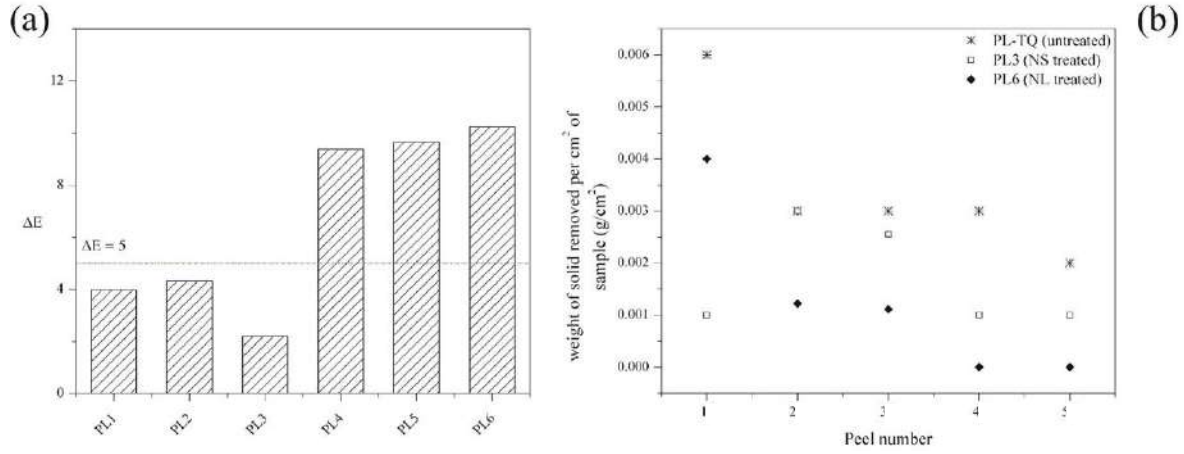

Fig. 2. (a) Colorimetric test results of treated samples; (b) Scotch tape test results of treated and untreated samples.

To get further information about the improvements that the NS/NL-protective layer exerts on limestone specimens, the water absorption coefficient (W_{ac}) for samples PL-TQ, PL3 and PL6 was also calculated, according to the UNI 10859 standard procedure [20]. The choice of these samples is justified by the occurrence that they are the only specimens for which the water absorption coefficient can be considered reliable. In fact, in the case of artificially aged samples, the presence of salts and/or humidity leads to visible alteration of the sample weights mostly due to the growth of salt crystals within the porous structure, instead of the presence of water.

Before the absorption test, weights of the dry samples were measured. Being the surface A of the sample in contact with water known, the amount of absorbed water per unit area Q_i at a time t_i can be calculated as:

$$Q_i = \frac{m_i - m_0}{A} \times 1000\,, \tag{6}$$

with m_i and m_0 equal to the mass (in grams) of the wet (measured at a time t_i after the water contact) and dry sample, respectively.

The amount of water absorbed per unit area by a porous solid, after the period of immersion t, can be considered simply proportional to the square root of time:

$$Q(t) = W_{ac}\sqrt{t}\,, \tag{7}$$

with W_{ac} equal to the aforementioned water absorption coefficient (g/(m^{2}s$^{0.5}$)).

The plot of $Q(t)$ vs. $\sqrt{t}$ for samples PL-TQ, PL3 and PL6 is reported in Fig. 3. All the curves show an initial linear trend (below 150 $s^{0.5}$), immediately followed by an asymptotic behavior, accounting for the full saturation of the specimen. The overall trend indicates a capillary network, dimensionally homogeneous and continuous or, in general, characterized by a good connection of the pores.

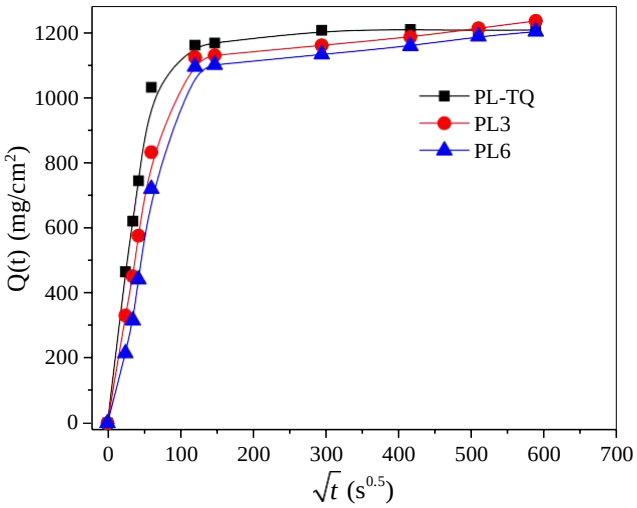

Fig. 3 $Q(t)$ vs. $\sqrt{t}$ plot for samples PL-TQ, PL3 and PL6. Continuous lines are guides for eyes.

According to Eq. 7, water absorption coefficients were evaluated from the slope of the linear part of curves displayed in Fig. 3, taking into account measurements up to 30 minutes, in agreement with the UNI 10859 standard procedure. The obtained values are 176.31 g/($m^2s^{0.5}$) for the reference sample (PL-TQ), 133.95 g/($m^2s^{0.5}$) for the sample treated with NS (PL3) and 100.31 g/($m^2s^{0.5}$) for the sample treated with NL (PL6). A slight decrease in the slope was experienced in both consolidated specimens, indicating a relative difficulty of water penetration, which can be attributed to a weak connection of the capillary pores or to heterogeneity in the distribution and/or dimensional variability of the porous network induced by both treatments.

Finally, the salt crystallization test was performed by means of partial immersion [23], based on standardized EN 12370:2001 procedure [24]. After just 24 h, efflorescences are noticeable on the surface of untreated sample as an effect of the migration of the saline solution. Conversely, in the consolidated samples, the efflorescences begin to be noticed around the 5-6 cycle. This is reasonably due to the evaporation rate of the solution at the surface of the stone, that could have been affected by the presence of the consolidant [30]. During the various cycles, increases and losses in weight up to the 15 cycle are evident in all samples regardless of the type of treatment. This occurrence can be explained taking into account that the location of salt crystallization is controlled by the water flow and the substrate permeability, that allows the salt to move. In fact, the formation of salt crystals usually generates significant internal stress or pressure for volume expansion [31,32]. If, on one side, the liquid phase allows salt to be transported, evaporation, outside or inside the material (i.e. efflorescence or subefflorescence, respectively), makes, on the other side, its crystallization possible [33]. After 15 cycles, specimens appear rounded, and the loss of small fragments is evident, mainly at the edges. Based on the obtained results and in agreement with [33], the observed variations (increasing and decreasing) in weight are the result of two phenomena occurring simultaneously, namely the development of efflorescence and subefflorescence, and the loss of material, although minimal, observed along the edges of the samples. (Fig. 4).

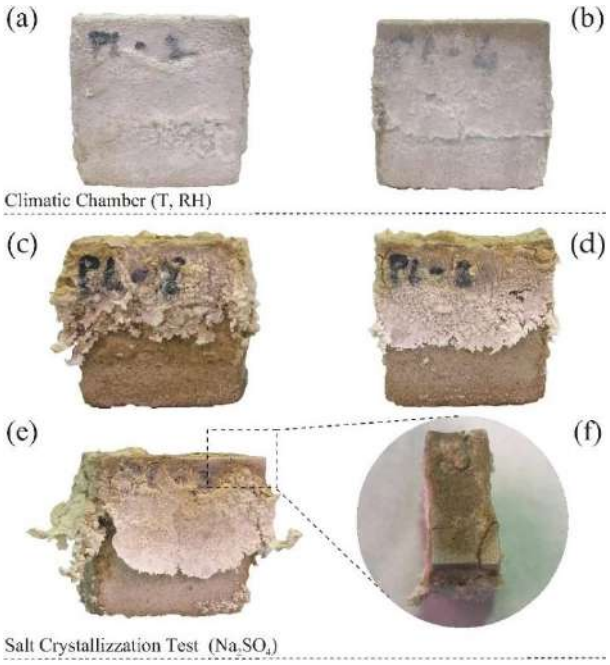

Fig. 4. (a,b) Macroscopic appearance of specimens aged by temperature and relative humidity chamber; (c) untreated specimen after salt crystallization test (15 cycles); (d,e) NS and NL treated specimen after salt crystallization test (15 cycles); (f) detail of small fragment detachment at the edges of the specimen after salt crystallization test.

Fig. 5 evidences, for all samples, an initial increase in weight (slightly greater for untreated sample), due to the entry of salt, prevailing over the loss by disintegration. After that, a relative progressive decrease in weight is detected, greater in the sample treated with NL [34,35]. This reduction in weight, although the efflorescences have been removed from the surface of the various specimens, does not allow the samples to reach the initial weight. This occurrence indicates that the observed increase is mainly due to the development of subefflorescences, and not to the loss of material or the presence of efflorescences.

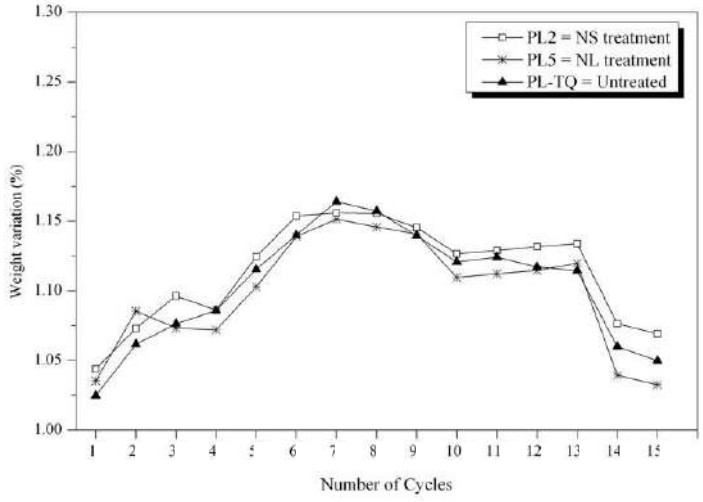

Fig. 5. Weight variation (%) for specimens subjected to salt crystallization test.

4.2. Neutron Radiography

Neutron images collected for sample PL6 at different selected time-steps and with an integration time of 10 s are displayed in Fig. 6, as example.

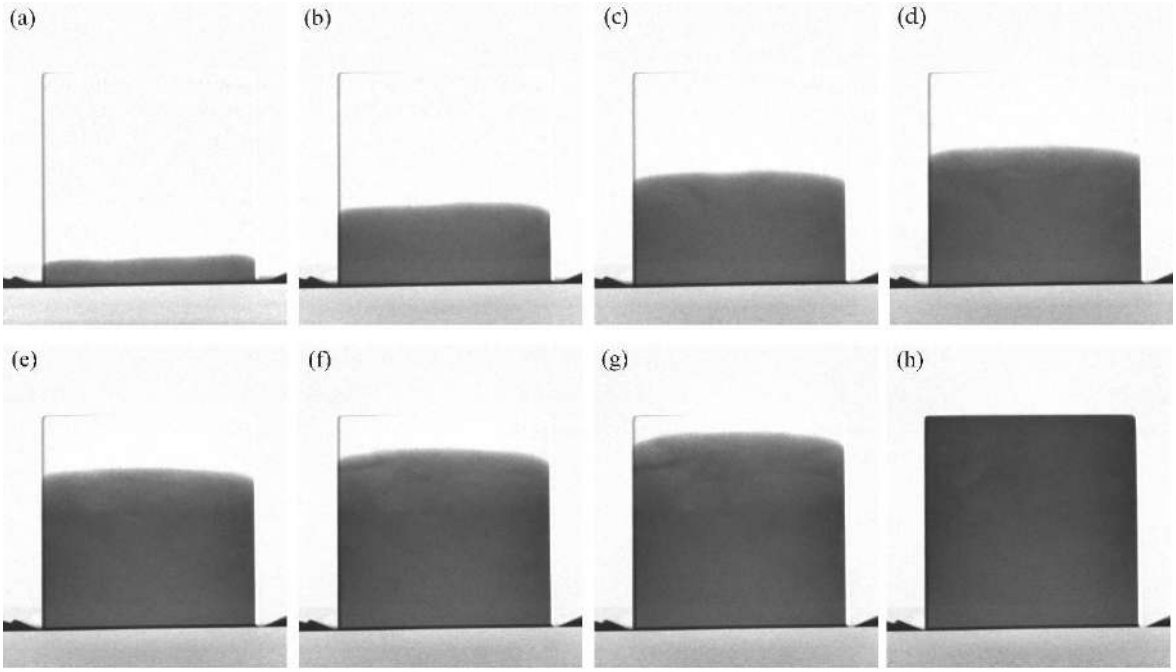

Fig. 6. Water penetration images of samples PL6, in which it's possible to follow the water front position as function of time: (a) 40 s; (b) 410 s; (c) 810 s; (d) 1210 s; (e) 1810 s; (f) 2040 s; (g) 2240 s; (h) saturation condition.

Thanks to the high quality of the obtained radiographs, the water penetration into the porous calcite-based materials can be clearly observed with high spatial and temporal resolution. The penetrating water front becomes visible for almost all the investigated samples after a contact time of 10 - 40 s, and goes towards the top of the stone with a regular rise until the full saturation of the specimen.
Going from the bottom to the top of the material, the water content decreases giving evidence of the presence of two distinct phases (water/stone) within the inner structure of the limestone during the imbibition. Furthermore, the formation of a well-defined boundary between the two aforementioned phases, as evidenced by the regularity of the water front at different contact times, experimentally supports the existence of a rather uniform microstructure without internal inhomogeneities, as already reported [17-19]. Finally, water is observed to flows up into the limestone specimen without any distortion of the path, testifying the absence of macroscopic (having size of the order of mm) watertight zones, that would be clearly visible in the NR images as light spots within the investigated ROI.
In Fig. 7 we report typical plots of water content (WC) as a function of the sample height for treated and untreated PL samples, as obtained for different contact times by scans performed in the first 30 min of exposure.

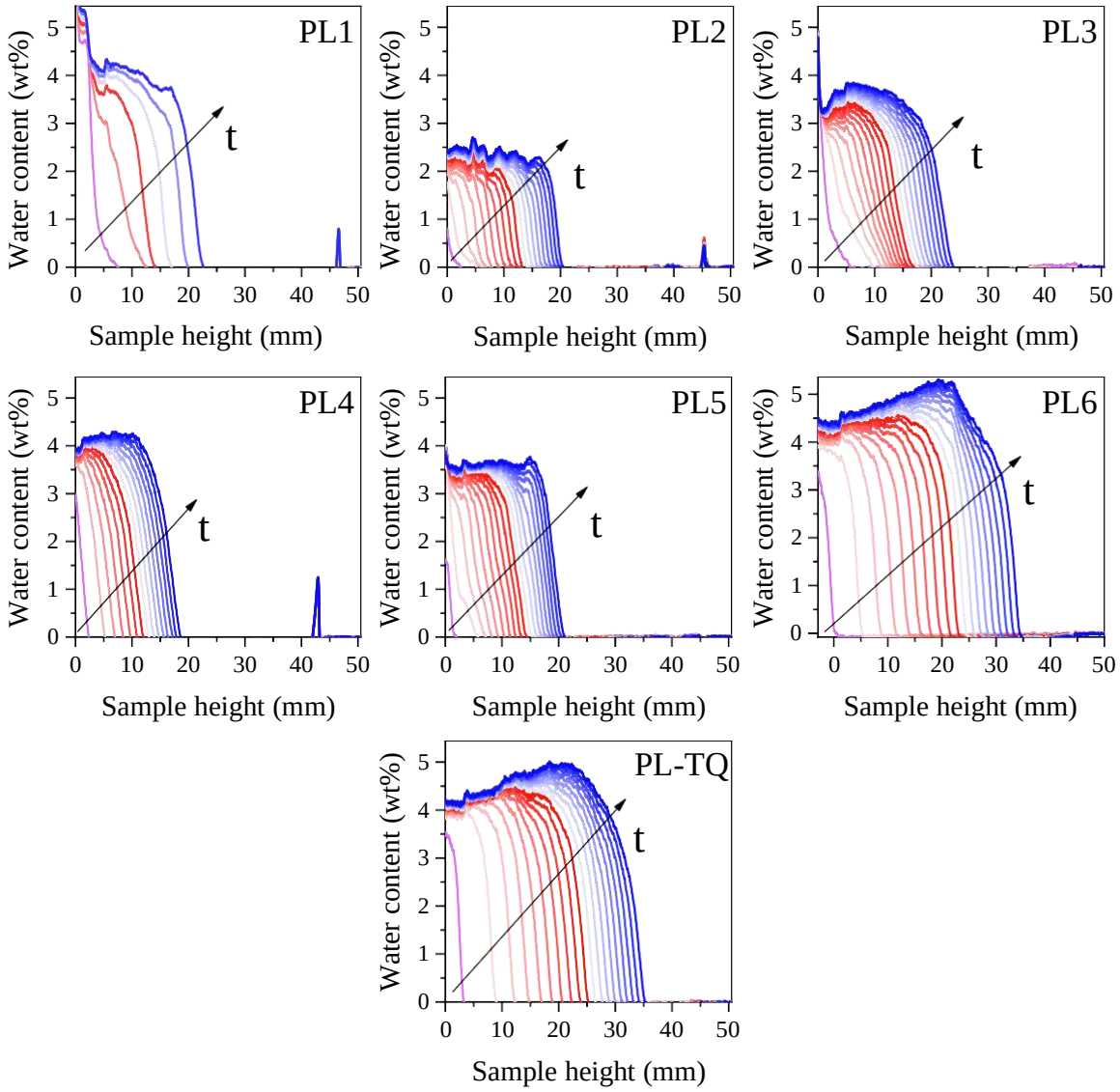

Fig. 7. Water content (WC) profiles as a function of the sample height for all investigated specimens. Plots are obtained for different contact times by scans performed in the first 30 min of exposure.

For all the investigated samples, the distance between two consecutive curves diminishes by increasing the contact time, indicating an accelerated water penetration rate in the first minutes of water absorption. This can be explained by taking into account both the initial available space for water inside the stone material and the porosity. In particular, even if the stone under investigation can be considered rather homogeneous [17-19], the observed diminishing could be justified in terms of a "skin" effect, widely reported in literature [36], according to which the outer layer of the stone appears significantly different from the inner ones (bulk) in terms of pore size distributions. Being the porosity much higher close to the surface of the stone, we shall expect more pronounced water suction by capillarity in the proximity of the outer shell, which slowly will tend to a plateau for long contact time, accounting the full saturation of the specimen. Furthermore, it is worth remarking that, according to the Young-Laplace equation [37], the capillary stresses are proportional to the inverse of the effective pore radius. Accordingly, a faster filling of small pores was expected, since larger cavities do not exert pressure enough to let the water flow up during the initial stage of contact.

Going on, it should be noticed that the obtained values for the water content and the height of water in the case of treated specimens, both artificially aged or not, are always lower than those of the untreated sample (PL-TQ), that were found to be ~ 5 wt% and ~ 35 mm, respectively. This occurrence

represents and experimental evidence of the consolidating action of both the used products. More in detail, the comparison of the wetting profiles of PL-TQ specimen with those calculated for the surface impregnated limestones not subjected to any artificial weathering test (PL3 and PL6) suggests that, in the early steps of the absorption test, the presence of nano-SiO_2 as consolidant clearly affects the water kinetics more than nanolime. In fact, after 30 min the suction motion into PL6, which was brushed with a ~ 2 mm thick layer of nanolime, turned out to be characterized by very similar values of WC and height of water. On the contrary, the water absorption for PL3 is more hindered of ~ 66.7%, reaching a maximum height of ~ 21 mm after 30 min. These preliminary results indicate that the use of nanosilica as a consolidating agent visibly affects the water uptake within the crystalline structure, presumably by occluding pores to a greater extent than nanolime. Concerning samples exposed to 15 cycles of salt crystallization, namely PL2 and PL5, a substantial reduction in the absorbed water can be observed. In particular, in the case of PL2 the water content turned out to be ~ 2.5 wt% after 30 min, reaching approximately ~ 18 mm of height in the sample, whereas a slight increase in the water content can be detected in PL5, reaching a value of ~ 3.5 wt% after the same time, and a penetration depth of ~ 20 mm. These results suggest that that the rising of water is more hindered in PL2 than in PL5 of ~ 28.6%, confirming the effectiveness of nanosilica as protective film in increasing the structural properties and hydrophobicity of the investigated limestone. Variations induced by thermal and RH treatment have also a measurable impact on the water absorption kinetics in PL limestones. In fact, in the case of PL1 and PL4 specimens, both consolidants seem to partially obstruct the water motion, as can be seen by the relatively low mean penetration depth reached by water in these two samples, with respect to PL-TQ. This can be reasonably due to an enlargement of the inner cavities induced by thenardite-mirabilite transition occurring as a consequence of changes in humidity and temperature [38]. In particular, the stone damage due to sodium sulfate is strictly related to the presence of these two different phases: because of the fluctuations in microclimatic conditions, the transition from thenardite to mirabilite is favored, and it is accompained by the development of high crystallization pressures [22,39].

In order to quantitatively determine the effect of the application of consolidants and artificial weathering tests on the water uptake process inside the analyzed stones, a classical theory of the water suction in porous materials has been taken into account [40,41]. Based on the model of "capillary transport" by J. R. Philip [42], widely reported in literature for a variety of homogeneous, porous materials including limestones [43,44], the wetted region obtained by neutron images was approximated to a fully saturated rectangular wet front. In our case, i.e. 1-phase flow and with constant air pressure, the mean penetration depth $x(t)$ can be predicted as a function of time using the following equation:

$$x(t) = S\sqrt{t} + B_0 t + B_1 t^{3/2} + \ldots, \quad (8)$$

being S the so-called sorptivity (m/s$^{0.5}$), considered as a measure of the tendency to absorb and transmit liquid through capillarity, and B_0 a dimensionless parameter known as *Bond number*, numerically equal to:

$$B_0 = (\rho K / \sigma) \times g\,. \quad (9)$$

In the above expression, ρ indicates the density of water (~ 1000 kg/m^3), K the intrinsic permeability of the rock (for limestone, permeability values range between 1.3×10^{-16} and 4×10^{-16} m^2 [45]), σ the air-water interfacial tension (~ 0.0729 N/m at T = 20 °C) and g the gravitational acceleration (~ 9.8 m/s^2). Based on these values, B_0 was found from Eq. 9 to be equal to ~ 1.34×10^{-11}. As a consequence, during the experiment the contribution of gravity can be neglected with respect to the active capillary forces [46]. In other words, for short time-steps the water suction can be considered only capillary-driven, being the effect of gravity too low at the initial stage to affect the water motion, and Eq. 8 reduces to:

$$x(t) = S\sqrt{t}\,. \tag{10}$$

According to literature [47-49], $x(t)$ was experimentally obtained through NR by looking at the sample height corresponding to the inflexion points (IPs) of the decreasing curves shown in Fig. 7, accounting for the wetting front position (WFP). The IPs account for the transition between a water-saturated region and a dried one (grey and white areas within the stone shown in Fig. 6). For all the investigated samples, as can be seen from an inspection of Fig. 7, the inflexion points correspond to water content of about 1 - 2 wt%.

In Fig. 8 we display the $x(t)$ vs. $\sqrt{t}$ plot for all the investigated PL samples at the initial stage of the water absorption process (first 30 min of exposure).

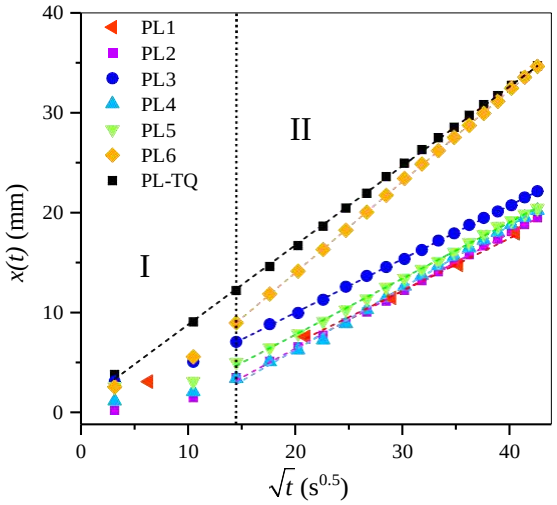

Fig. 8. $x(t)$ vs. $\sqrt{t}$ plot, as obtained from NR analysis, for all the investigated PL samples.

First of all, it is worth of note that in the case of PL-TQ specimen, if compared to the treated PL samples, a favored water penetration is clearly observed. This can be due to the fact that since no protective coating is applied, an initial bottom swelling could occur, making the structure more susceptible to the presence of water, especially during the first minutes of exposure.
Based on Eq. 10, a linear dependence on $t^{0.5}$ was expected for the mean penetration depth, also according to what already reported in literature for uniform bricks, mortars and limestones [50-53]. Actually, for all the investigated specimens, with the exception of PL-TQ for which a linear trend is revealed, a non-linear dependence on $t^{0.5}$ can be observed during the first 4 minutes of exposure ($\sqrt{t}$ < ~ 15 $s^{0.5}$), followed by the expected linear trend. This occurrence suggests the presence of two regions characterized by different water suction kinetics, namely region I and region II. According to Küntz and Lavallèe [54], a possible explanation for this different absorption behavior could be a deviation from the water flux gradient proportionality accounted by the Darcy's Law. Moreover, a not uniform capillary force during the water absorption, due to an intrinsic anisotropy of the stone, may also contribute to deviation from the theoretical model [55,56]. In our case, for treated samples it is reasonable to assume that, at the initial stage of the water absorption process (region I), the crossing of the NS/NL-protective layers by water after the initial contact can be responsible of the observed deviation from the theoretical model. In fact, the presence of consolidants brushed onto the limestone surface tends to change the chemical-mechanical properties of the stone outer layers, leading to significant variations in the effective pores' distribution. This leads the system towards a less homogeneous conformation characterized by two types of porosity, the first one associated to the stone + consolidant system (limited to the impregnated thickness) and the second one related to the

rest of the stone. As a consequence, the assumption at the basis of the model, consisting in dealing with homogenous, porous materials, is not valid any more. However, after a short period of time, the observed variation in the water absorption tendency, accounted by the residual linear-dependent part of the calculated depth profiles vs. $t^{0.5}$ (region II), can be associated to the presence of a greater pore volume made up of air bubbles of ~ 0.5 - 4 μm available for the water flow inside the inner stone microstructure [57].

In order to quantitatively evaluate the susceptibility to weathering of the investigated materials, the sorptivity S was evaluated by linear fit (according to Eq. 10) of the WFPs in region II, as reported in Fig. 8.

The obtained S values in PL samples are reported in Table 2. As can be seen, they range from 9.13×10^{-4} m/s$^{0.5}$ (PL6) to 5.27×10^{-4} m/s$^{0.5}$ (PL1), that corresponds to a relative variation of ~ 73.2%.

Sample	S (m/s$^{0.5}$)
PL1	5.27×10^{-4}
PL2	5.78×10^{-4}
PL3	5.37×10^{-4}
PL4	6.21×10^{-4}
PL5	5.63×10^{-4}
PL6	9.13×10^{-4}
PL-TQ	8.03×10^{-4}

Table 2. Sorptivity values calculated for all the investigated specimens through linear fit of the water front position as a function of the square root of time.

Such a difference can be attributed to several factors, including distribution of pores inside the stone matrix and artificial ageing treatments. Let's focus first of all the attention on values obtained for PL-TQ specimen, and for samples consolidated but not artificially aged, namely PL3 (consolidated with NS) and PL6 (consolidated with NL). In the case of PL-TQ limestone, the tendency to absorb and transmit water by capillary suction is expressed by an S -value of 8.03×10^{-4} m/s$^{0.5}$, which is higher than, or at least equal to, the values obtained for the specimens treated with the two protective layers. In particular, the value of S for PL6 (9.13×10^{-4} m/s$^{0.5}$) appears almost comparable to that of PL-TQ, which means that during the initial stage of the water uptake the presence of nanolime brushed onto the surface does not affect almost at all the water absorption tendency. This can be explained considering the possible effect that NL exerts on the 3D microstructure of the investigated stone. As a matter of fact, it can reasonably hypothesized that the use of NL increases the water fluidity. This because this product does not occlude pores but rather reinforces them. As a consequence, the rise of the water front is not significantly hindered, being the microstructure close the surface almost "open" for the capillary suction process. Moreover, as evidenced by Al-Omary et. al. [58], the variation of the pores distribution induced by nanolime in limestone specimens is almost negligible, and hence the water absorption cannot be considerably affected by a different porosity. Finally, the limited impact of NL can be also ascribed to a relatively low penetration depth of such consolidant into the limestone structure.

On the contrary, the sorptivity calculated in the case of PL3 (5.37×10^{-4} m/s$^{0.5}$) appears decreased by 47.1% with respect to reference specimen, suggesting a partial occlusion of the outer layer pores caused by the presence of the consolidant. As a result, the water rise in the first 30 minutes of contact is strongly hindered, which confirms that the use of Nano Estel® (nano-SiO_2) as protective product against short-term weathering agents is much more convenient with respect to CaLoSiL® (nanolime).

Regarding the kinetics associated to the initial stage of water suction for artificially aged samples treated with nanosilica (PL1 and PL2) or nanolime (PL4 and PL5), we can state that the comparable S values obtained for, on one side, PL1 (5.27×10^{-4} m/s$^{0.5}$) and PL4 (6.21×10^{-4} m/s$^{0.5}$) and, on the other side, PL2 (5.78×10^{-4} m/s$^{0.5}$) and PL5 (5.63×10^{-4} m/s$^{0.5}$) suggest that the type of treatment do not significantly affect the water absorption tendency of stones subjected to thermal/RH stresses and/or 15 cycles of salt crystallization.

It is worth of note, however, that both solutions (NL and NS) seem to act as stabilizers against artificial aging, as revealed by the obtained lower values of sorptivity with respect to that calculated

for PL-TQ. This occurrence could be related both to the intrinsic heterogeneity of each specimen and to an increase, because of the treatment and the aging, in the volume of the pores with capillary activity at the expenses of the coarser pores. In other words, the treatment is supposed to produce a change in the pore size distribution, limited to the impregnated thickness. Depending on the quantity of product that enters the porous network, variations in the pores distribution can occur. At the same time, the connectivity degree of the pores can be changed following salt crystallization. The salt may, in fact, completely occlude the smaller pores (with greater capillary activity) and only partially the larger ones.

For a better understanding of the effect that temperature/RH jumps and salt crystallization cycles induce into the NS- and NL-treated samples, the time t_{sat} needed to reach the water saturated condition was also accounted.

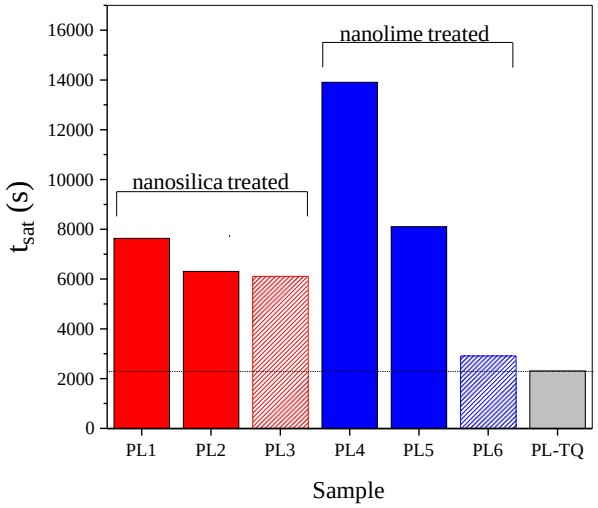

Fig. 9. t_{sat} values calculated for all the PL samples. More in detail, red and blue closed bars refer to the artificially aged samples treated with nanosilica (PL1 and PL2) and nanolime (PL4 and PL5), whereas red and blue hatched bars refer to the only-treated samples not subjected to any artificial weathering test (PL3 and PL6, consolidated by NS and NL respectively). Grey closed bar refers to PL-TQ, used as reference.

As can be seen, the saturation times for PL3 and PL6 are higher than that of PL-TQ, which means that both NL and NS consolidants keep the system strongly hydrophobic.

As already stated, the use of nanosilica as hampering agent against water penetration seems to be more convenient with respect to nanolime. This is also reflected in the time needed to reach the saturation state, as reported in Fig. 9. In fact, in the case of sample PL3 t_{sat} was found to be higher (~ 6110 s) than that of PL6 (~ 2900 s), revealing a hindering in water absorption process also for longer exposure time. As far as PL6 and PL-TQ are concerned, the saturation times seem to be almost comparable, suggesting a similar water soaking tendency of the two samples, in agreement with what already revealed from the sorptivity analysis.

Going on, limestones subjected to thermal/RH stresses after 3 cycles of salt crystallization (PL1 and PL4) are characterized by higher saturation times with respect to those exposed to 15 cycles of salt crystallization (PL2 and PL5). This can be explained by considering that, in the latter case, artificial weathering will presumably lead to fractures, cracks and plane distortions to a greater extent than those caused by the thenardite-mirabilite transition induced by changes in humidity and temperature. These features can be considered as preferential pathways for liquid water, which means that water can now penetrate more efficiently within the stone network and reach the top of the specimen more quickly, regardless of the type of treatment used.

On the other side, thermal and/or RH stresses can probably give rise to an enlargement of the initial micro-cracks of the stone, causing an irreversible structural damage and reducing the intra-cavity

distances. This will imply, in agreement with the Young-Laplace equation [37], a delay in reaching saturation conditions.

From the whole set of neutron radiography results, the use of nanosilica is found to partially hinder the pores of the outer layers, without fulfill them, in a more efficient way with respect to nanolime. Although the calculated water absorption coefficients do not seem to fully support this statement, this small discrepancy can be explained considering that, first of all, the penetration of NL and NS may be different during the laboratory and NR measurements. At the same time, the hampering effect of the two treatments with respect to water may not be the same. Furthermore, assuming a proper inclusion of the consolidants within the porous structure of the investigated stones, the penetration depth of the two products may be different, giving rise to different water diffusion properties especially at the initial stage of the water absorption process.

Finally, it is also worth remarking that an almost-open microstructure, as observed for nanolime consolidated limestones, is anyway of relevance in material science, since in this case the elastic modulus and the thermal expansion coefficient of the rock are not altered in substantial way, and water transport by capillary suction is still possible.

5. Conclusions

In this work, a systematic neutron radiography investigation on *Pietra di Lecce* limestone, widely employed as building material in Lecce city (Puglia, Southern Italy), was performed. The aim was to provide an evidence of the effectiveness of two different commercially-available consolidants (i.e. nanosilica and nanolime) as protective agents against several artificial weathering tests. The obtained neutron radiographs allowed us to visualize, in a non-destructive way, the water motion inside the investigated limestones, which was used as marker for the study of the water absorption/petrophysical properties. A close relationship between structure, texture and composition of the rock and its behaviour, in terms of response to degradation, was demonstrated. The qualitative and quantitative analysis of the maximum amount of absorbed water, wetting front position and saturation times, revealed an overall better performance of nanosilica with respect to nanolime, even if slight changes in the capillary transport kinetics of aqueous solutions were highlighted. The effects of artificial weathering on the pores network were also evidenced, suggesting the formation of new channels, plane distortions and cracks, associated to the strong crystallization pressure experienced by the structure as a result of phase transitions induced by artificial microclimatic variations.

As final remark, we want to underlying that the results reported here can be used as a methodological proposal scheme, to be defined from time to time, for selecting and designing the proper procedure to be adopted in order to preserve and maintain buildings/objects of interest in the field of cultural heritage and conservation science.

References

[1] M.F. La Russa, G. Barone, C.M. Belfiore, P. Mazzoleni, A. Pezzino, Application of protective products to “Noto” calcarenite (south-eastern Sicily): a case study for the conservation of stone materials, Environ. Earth Sci. 62 (2010) 1263-1272. https://doi.org/10.1007/s12665-010-0614-3.

[2] C. Bottari, G.M. Crisci, V. Crupi, V. Ignazzitto, M.F. La Russa, D. Majolino, M. Ricca, B. Rossi, S.A. Ruffolo, J. Teixeira, V. Venuti, SANS investigation of the salt-crystallization- and surface-treatment-induced degradation on limestones of historic–artistic interest, Appl. Phys. A - Mater. 122 (2016) 721-730. https://doi.org/10.1007/s00339-016-0252-z.

[3] V. Crupi, B. Fazio, A. Gessini, Z. Kis, M.F. La Russa, D. Majolino, C. Masciovecchio, M. Ricca, B. Rossi, S.A. Ruffolo, V. Venuti, TiO2–SiO2–PDMS nanocomposite coating with self-cleaning effect for stone material: Finding the optimal amount of TiO2, Constr. Build. Mater. 166 (2018) 464-471. https://doi.org/10.1016/j.conbuildmat.2018.01.172.

[4] V. Cnudde, M. Dierick, J. Vlassenbroeck, B. Masschaele, E. Lehmann, P. Jacobs, L. Van Hoorebeke, Determination of the impregnation depth of siloxanes and ethylsilicates in porous material by neutron radiography, J. Cult. Herit. 8 (2007) 333-338. https://doi.org/10.1016/j.culher.2007.08.001

[5] B. Doherty, M. Pamplona, C. Miliani, M. Matteini, A. Sgamellotti, B. Brunetti, Durability of the artificial calcium oxalate protective on two Florentine monuments, J. Cult. Herit. 8 (2007) 186-192. https://doi.org/10.1016/j.culher.2006.12.002.
[6] C. Hall, T.K.M. Tse, Water-movement in porous building materials-VII. The sorptivity of mortars, Build. Environ. 21 (1986) 113–118. https://doi.org/10.1016/0360-1323(86)90017-X.
[7] J. Kaufmann, W. Studer, J. Link, K. Schenker, Study of water suction of concrete with magnetic resonance imaging methods, Magazine Concrete Res. 49 (1997) 157–165. https://doi.org/10.1680/macr.1997.49.180.157.
[8] G. Barone, V. Crupi, D. Majolino, P. Mazzoleni, J. Teixeira, V. Venuti, Small angle neutron scattering as fingerprinting of ancient potteries from Sicily (Southern Italy), J. Appl. Phys. 106 (2009) 054904. https://doi.org/10.1063/1.3204020.
[9] G. Barone, V. Crupi, F. Longo, D. Majolino, P. Mazzoleni, S. Raneri, J. Teixeira, V. Venuti, Neutron radiography for the characterization of porous structure in degraded building stones, J. Instrum. 9 (2014) C05024. https://doi.org/10.1088/1748-0221/9/05/C05024.
[10] G. Barbera, G. Barone, V. Crupi, F. Longo, G. Maisano, D. Majolino, P. Mazzoleni, S. Raneri, J. Teixeira, V. Venuti, A multi-technique approach for the determination of the porous structure of building stone, Eur. J. Mineral. 26 (2014) 189-198. doi:10.1127/0935-1221/2014/0026-2355.
[11] V. Cnudde, T. De Kock, M. Boone, W. De Boever, T. Bultreys, J. Van Stappen, D. Vandevoorde, J. Dewanckele, H. Derluyn, V. Cardenes, L. Van Hoorebeke, Conservation studies of cultural heritage: X-ray imaging of dynamic processes in building materials, Eur. J. Mineral. 27 (2015) 269-278. https://doi.org/10.1127/ejm/2015/0027-2444.
[12] M. Realini, C. Colombo, C. Conti, F. Grazzi, E. Perelli Cippo, J. Hovind, Development of neutron imaging quantitative data treatment to assess conservation products in cultural heritage, Anal. Bioanal. Chem. 409 (2017) 6133-6139. https://doi.org/10.1007/s00216-017-0550-0.
[13] M. Lanzón, V. Cnudde, T. De Kock, J. Dewanckele, A. Piñero, X-ray tomography and chemical-physical study of a calcarenite extracted from a Roman quarry in Cartagena, (Spain), Eng. Geol. 171 (2014) 21-30. https://doi.org/10.1016/j.enggeo.2013.12.007.
[14] M.F. La Russa, C.M. Belfiore, G.V. Fichera, R. Maniscalco, C. Calabrò, S.A. Ruffolo, A. Pezzino, The behaviour to weathering of the Hyblean limestone in the Baroque architecture of the Val di Noto (SE Sicily): an experimental study on the “calcare a lumachella” stone, Constr. Build. Mater. 7 (2015) 7-19. https://doi.org/10.1016/j.conbuildmat.2014.11.073.
[15] A. Calia, M. Laurenzi Tabasso, A.M. Mecchi, G. Quarta, The study of stone for conservation purposes: Lecce stone (southern Italy), Geol. Soc. Spec. Publ. 391 (2013) 139-156. https://doi.org/10.1144/SP391.8.
[16] S. Bugani, M. Camaiti, L. Morselli, E. Van de Casteele, K. Janssens, Investigation on porosity changes of Lecce stone due to conservation treatments by means of x-ray nano- and improved micro-computed tomography: preliminary results, X-Ray Spectrom. 36 (2007) 316-320. https://doi.org/10.1002/xrs.976.
[17] R.J. Dunham, Classification of carbonate rocks according to depositional texture. In: Ham W.E. (Ed.), Classification of carbonate rocks, Am. Assoc. Petrol. Geol. Memo, 1962, pp. 108–21.
[18] F. Zezza, Le pietre da costruzione e ornamentali della Puglia. Caratteristiche sedimentologiche petrografiche, proprietà fisiche e meccaniche e problemi geologico tecnici relativi all’attività estrattiva, Rass. Tecn. Pugliese, 1974, n. 3-4.
[19] U. Zezza, F. Veniale, F. Zezza, G. Moggi, Effetti dell’imbibizione sul decadimento meccanico della pietra leccese, in: Proceedings of the 1st International Symposium for the Conservation of Monuments in the Mediterranean Basin, 1989, pp. 263-269.
[20] UNI 10859:2000, Beni culturali - Materiali lapidei naturali ed artificiali - Determinazione dell'assorbimento d'acqua per capillarità (2000).
[21] M. Drdácký, J. Lesák, S. Rescic, Z. Slížková, P. Tiano, J. Valach, Standardization of peeling test for assessing the cohesion and consolidation characteristics of historic stone surfaces, Mater. Struct. 45 (2012) 505-520. https://doi.org/10.1617/s11527-011-9778-x.
[22] C. Rodriguez-Navarro, E. Doehne, E. Sebastian, How does sodium sulfate crystallize? implications for the decay and testing of building materials, Cement Concrete Res. 30 (2000) 1527-1534. https://doi.org/10.1016/S0008-8846(00)00381-1.

[23] D. Benavente, M.A. Garcı´a del Cura, A. Bernabéu, S. Ordóñez, Quantification of salt weathering in porous stones using an experimental continuous partial immersion method, Eng. Geol. 59 (2001) 313-325. https://doi.org/10.1016/S0013-7952(01)00020-5.
[24] EN 12370 Natural stone test methods-determination of resistance to salt crystallization. European Committee for Standardization (CEN), Brussels, (2001) 108-121.
[25] J. Dewanckele, T. De Kock, G. Fronteau, H. Derluyn, P. Vontobel, M. Dierick, L. Van Hoorebeke, P. Jacobs, V. Cnudde, Neutron radiography and X-ray computed tomography for quantifying weathering and water uptake processes inside porous limestone used as building material, Mater. Charact. 88 (2014) 86–99. https://doi.org/10.1016/j.matchar.2013.12.007.
[26] J. Schindelin, I. Arganda-Carreras, E. Frise, V. Kaynig, M. Longair, T. Pietzsch, S. Preibisch, C. Rueden, S. Saalfeld, B. Schmid, J.-Y. Tinevez, D.J. White, V. Hartenstein, K. Eliceiri, P. Tomancak, A. Cardona, Fiji - an Open Source platform for biological image analysis, Nat. Methods 9 (2012) 676-682. https://doi.org/10.1038/nmeth.2019.
[27] F.H. Kim, D. Penumadu, D.S. Hussey, Water distribution variation in partially saturated granular materials using neutron imaging, J. Geotech. Geoenviron. Eng. 138 (2012) 147-154. http://dx.doi.org/10.1061/(ASCE)GT.1943-5606.0000583.
[28] Normal 43/93: Misure colorimetriche di superfici opache. Roma CNR, 1993.
[29] R.F. Witzel, R.W. Burnham, J.W. Onley, Threshold and suprathreshold perceptual color differences, J. Opt. Soc. Am. 63 (1973) 615-625. https://doi.org/10.1364/JOSA.63.000615.
[30] M.F. La Russa, S.A. Ruffolo, M.Á. de Buergo, M. Ricca, C.M. Belfiore, A. Pezzino, G.M. Crisci, The behaviour of consolidated Neapolitan yellow Tuff against salt weathering, Bull. Eng. Geol. Environ. 76 (2017) 115-124. https://doi.org/10.1007/s10064-016-0874-6.
[31] I.S. Evans, Salt crystallization and rock weathering: a review, Revue Geomorph. Dynam. 19 (1970) 153-177.
[32] D. Benavente, J. Martínez-Martínez, N. Cueto, M.A. García-del-Cura, Salt weathering in dual-porosity building dolostones, Eng. Geol. 94 (2007) 215-226. https://doi.org/10.1016/j.enggeo.2007.08.003.
[33] G. Cultrone, E. Sebastián, Laboratory simulation showing the influence of salt efflorescence on the weathering of composite building materials, Environ. Geol. 56 (2008) 729-740. https://doi.org/10.1007/s00254-008-1332-y.
[34] D. Benavente, M.A. Garcı´a del Cura, R. Fort, S. Ordóñez, Durability estimation of porous building stones from pore structure and strength, Eng. Geol. 74 (2004) 113-127. https://doi.org/10.1016/j.enggeo.2004.03.005.
[35] D. Benavente, M.A. Garcı´a del Cura, S. Ordóñez, Salt influence on evaporation from porous building rocks, Constr. Build. Mater. 17 (2003) 113-122. https://doi.org/10.1016/S0950-0618(02)00100-9.
[36] T. Zhao, G. Zhu, F.H. Wittmann, W. Li, On surface impregnation of chloride contaminated cement based materials, in: Proc. 5th Int. Conf. on Water Repellent Treatment of Building Materials, Hydrophobe V 5 (2008) 311-324.
[37] C.L. Lucero, D.P. Bentz, D.S. Hussey, D.L. Jacobson, W.J. Weiss, Using neutron radiography to quantify water transport and the degree of saturation in entrained air cement based mortar, Phys. Procedia 69 (2015) 542-550. https://doi.org/10.1016/j.phpro.2015.07.077.
[38] M. Steiger, S. Asmussen, Crystallization of sodium sulfate phases in porous materials: The phase diagram Na2SO4-H2O and the generation of stress, Geochim. Cosmochim. Acta 72 (2008) 4291-4306. https://doi.org/10.1016/j.gca.2008.05.053.
[39] N. Tsui, R.J. Flatt, G.W. Scherer, Crystallization damage by sodium sulfate, J. Cult. Herit. 4 (2003) 109-115. https://doi.org/10.1016/S1296-2074(03)00022-0.
[40] D. Kirkham, W.L. Powers, Advanced Soil Physics, Wiley, New York, 1972.
[41] F. Dullien, Porous Media. Fluid Transport and Pore Structure, first ed., Academic Press, New York, 1979.
[42] J.R. Philip, Theory of infiltration, Adv. Hydroscience 5 (1969) 215-296. https://doi.org/10.1016/B978-1-4831-9936-8.50010-6.
[43] N. Alderete, Y. Villagrán Zaccardi, D. Snoeck, B. Van Belleghem, P. Van den Heede, K. Van Tittelboom, N. De Belie, Capillary imbibition in mortars with natural pozzolan, limestone powder

699 and slag evaluated through neutron radiography, electrical conductivity, and gravimetric analysis,
700 Cement Concrete Res. 118 (2019) 57-68. https://doi.org/10.1016/j.cemconres.2019.02.011.
701 [44] I. Ioannou, A. Andreou, B. Tsikouras, K. Hatzipanagiotou, Application of the sharp front model
702 to capillary absorption in a vuggy limestone, Eng. Geol. 105 (2009) 20-23.
703 https://doi.org/10.1016/j.enggeo.2008.12.008.
704 [45] Z. Lafhaj, G. Richard, M. Kaczmarek, F. Skoczylas, Experimental determination of intrinsic
705 permeability of limestone and concrete: comparison between in situ and laboratory results, Build.
706 Environ. 42 (2007) 3042–3050. https://doi.org/10.1016/j.buildenv.2006.07.039.
707 [46] C.L. Cheng, E. Perfect, B. Donnelly, H.Z. Bilheux, A.S. Tremsin, L.D. McKay, V.H. DiStefano,
708 J.C. Cai, L.J. Santodonato, Rapid imbibition of water in fractures within unsaturated sedimentary
709 rock, Adv. Water Resour. 77 (2015) 82–89. http://dx.doi.org/10.1016/j.advwatres.2015.01.010.
710 [47] P. Zhang, F.H. Wittmann, T.J. Zhao, E. Lehmann, Observation and quantification of water
711 penetration into frost damaged concrete by neutron radiography, Restoration of Buildings and
712 Monuments 16 (2010) 195-210. https://doi.org/10.1515/rbm-2010-6373.
713 [48] V. Cnudde, M. Dierick, J. Vlassenbroeck, B. Masschaele, E. Lehmann, P. Jacobs, L. Van
714 Hoorebeke, High-speed neutron radiography for monitoring the water absorption by capillarity in
715 porous materials, Nucl. Instrum. Methods Phys. Res. B 266 (2008) 155-163.
716 https://doi.org/10.1016/j.nimb.2007.10.030.
717 [49] M. Luković, G. Ye, E. Schlangen, K. van Breugel, Moisture movement in cement-based repair
718 systems monitored by X-ray absorption, Heron 62 (2017) 21-45.
719 [50] L. Yang, D. Gao, Y. Zhang, J. Tang, Y. Li, Relationship between sorptivity and capillary
720 coefficient for water absorption of cement-based materials: theory analysis and experiment, R.
721 Soc. open sci. 6 (2019) 190112. http://dx.doi.org/10.1098/rsos.190112.
722 [51] D. Małaszkiewicz, J. Chojnowski, Influence of addition of calcium sulfate dihydrate on drying of
723 autoclaved aerated concrete, Open Eng. 7 (2017) 273-278. https://doi.org/10.1515/eng-2017-0032.
724 [52] A.E. Abd, J.J. Milczarek, Neutron radiography study of water absorption in porous building
725 materials: anomalous diffusion analysis, J. Phys. D: Appl. Phys. 37 (2004) 2305–2313.
726 https://dx.doi.org/10.1088/0022-3727/37/16/013.
727 [53] L. Hanzic, R. Ilic, Relationship between liquid sorptivity and capillarity in concrete, Cement
728 Concrete Res. 33 (2003) 1385–1388. https://doi.org/10.1016/S0008-8846(03)00070-X.
729 [54] M. Kuntz, P. Lavallée, Experimental evidence and theoretical analysis of anomalous diffusion
730 during water infiltration in porous building materials, J. Phys. D: Appl. Phys. 34 (2001) 2547–
731 2554. https://doi.org/10.1088/0022-3727/34/16/322.
732 [55] A. Brú, J.M. Pastor, Experimental characterization of hydration and pinning in bentonite clay, a
733 swelling, heterogeneous, porous medium, Geoderma 134 (2006) 295–305.
734 https://doi.org/10.1016/j.geoderma.2006.03.006.
735 [56] J. Cai, B. Yu, A discussion of the effect of tortuosity on the capillary imbibition in porous media,
736 Transp. Porous Media 89 (2011) 251–263. https://doi.org/10.1007/s11242-011-9767-0.
737 [57] M.I. Gomes, T.D. Gonçalves, P. Faria, Hydric behavior of earth materials and the effects of their
738 stabilization with cement or lime: study on repair mortars for historical rammed earth structures, J.
739 Mater. Civil Eng. 28 (2016) 04016041. https://doi.org/10.1061/(ASCE)MT.1943-5533.0001536.
740 [58] R.A. Al-Omary, M. Al-Naddaf, W. Al Sekhaneh, Laboratory evaluation of nanolime
741 consolidation of limestone structures in the Roman site of Jerash, Jordan, Mediterr. Archaeol.
742 Archaeom. 18 (2018) 35-43. https://doi.org/10.5281/zenodo.1323865.